Classical and Nonclassical Nucleation and Growth Mechanisms for Nanoparticle Formation

Young-Shin Jun*, Yaguang Zhu, Ying Wang, Deoukchen Ghim, Xuanhao Wu§, Doyoon Kim‡, and Haesung Jung‡

Department of Energy, Environmental and Chemical Engineering,

Washington University in St. Louis, St. Louis, MO 63130

*Corresponding Author: Young-Shin Jun ORCID: 0000-0003-4648-2984;

Address: One Brookings Drive, Campus Box 1180

E-mail: <u>ysjun@wustl.edu</u>

Phone: (314)935-4539

Fax: (314)696-1223

http://encl.engineering.wustl.edu/

Mr. Yaguang Zhu, Telephone: (314) 295-0196, E-mail: yaguangzhu@wustl.edu, ORCID 0000-0002-1522-4491

Ms. Ying Wang, Telephone: (314) 480-2501, Email: w.ying@wustl.edu,

ORCID: 0000-0001-8778-364X

Mr. Deoukchen Ghim, Telephone: 314) 640-6447, E-mail: dghim@wustl.edu, ORCID: 0000-0003-2041-5820

Dr. Xuanhao Wu, Telephone: (314) 250-8558, E-mail: xuanhao.wu@yale.edu, ORCID: 0000-0001-6177-6089

Dr. Doyoon Kim, Telephone: (314) 761-7049, E-mail: doyoon@wustl.edu, ORCID: 0000-0001-9496-5556

Dr. Haesung Jung, Telephone: 82 (055) 213-3756, Email: haesung.jung@changwon.ac.kr, ORCID: 0000-0002-8795-248X

Volume 73 of the Annual Review of Physical Chemistry

Submitted: September 2021

Current addresses

- § Department of Chemical and Environmental Engineering, Yale University, New Haven, CT 06511, USA
- ‡ Department of Civil and Environmental Engineering, Massachusetts Institute of Technology, Cambridge, MA 02139, USA
- ‡ School of Civil, Environmental and Chemical Engineering, Changwon National University, Changwon, Gyeongsangnam-do, 51140, South Korea

Abstract

All solid materials are created *via* nucleation. In this evolutionary process, nuclei form in solution

or at interfaces and expand by monomeric growth, oriented attachment, and phase transformation.

Nucleation determines the location and size of nuclei, while growth controls the size, shape, and

aggregation of newly formed nanoparticles. These physical properties of nanoparticles can

determine their functionalities, reactivities, and porosities, as well as their fate and transport.

Recent advances in nanoscale analytical technologies allow in situ real-time observations, enabling

us to uncover the molecular nature of nuclei and the critical controlling factors for nucleation and

growth. While a single theory cannot yet fully explain such evolving processes, we have started to

better understand how both classical and non-classical theories can work together, and we have

begun to recognize the importance of connecting these theories. This review discusses the recent

convergence of knowledge about the nucleation and the growth of nanoparticles.

Keywords: Classical Nucleation Theory, Non-classical Nucleation Theory, Crystal Growth,

Oriented Attachment, Phase Transformation, Interfacial Structure

1

1. Introduction

The nucleation and growth of nanoparticles play vital roles in such research fields as chemistry (1; 2), geology (3-6), biology (7; 8), physics (9), materials science (10; 11), and environmental remediation (12-14). In the natural environment, changes in the reactive surface area during mineral nucleation and growth create heterogeneities in the mineral phase and texture in sediments and soils (3). In particular, iron and manganese (hydr)oxides form ubiquitously and act as both natural electron donors and acceptors, contributing to geochemical redox cycling (4-6) and affecting the fate and transport of heavy metals and other toxic anions (14). In the atmosphere, the nucleation of sub-2 nm clusters of atmospheric aerosols and their growth can significantly affect direct/indirect radiative forcing, altering climate (1). In engineered environmental systems, the nucleation and growth of calcium carbonate, calcium sulfate, and barium sulfate cause scaling in membrane desalination systems and oil pipelines (12; 13). In biological systems, macromolecules in organisms direct nanocrystal nucleation and growth to build vertebrate skeletal systems (i.e., calcium phosphate mineral formation with collagen), mollusk shells, and other rigid biological structures (7; 8). In materials design and transformative manufacturing, controlling the nucleation and growth of nanocrystals is critical to achieving on-demand sizes, crystal structures, and shapes with unique optical, electrical, thermal, and mechanical properties (10; 11). Because of the immense importance of solid nucleation and growth, the last few decades have seen much new experimental research and a variety of diverse interpretations of its findings. Now we face the important task of connecting the advanced understanding of these systems gained from experimental results with a robust theoretical framework that integrates both classical and nonclassical nucleation and growth mechanisms.

This review presents the current experimental understanding of the nucleation and growth of nanoparticles and the theoretical approaches to describe these processes. It focuses on the solid nucleation and growth of solids from solution rather than on liquid condensation from the gas phase or new solid nucleation from pre-existing solids. First, the review highlights advanced experimental approaches that provide high spatiotemporal resolution, which enable observations or quantifications of the nucleation and growth of nanoparticles (Section 2). Second, we introduce classical and non-classical nucleation and growth theories, recent experimental findings, and their relation to these theories (Sections 3-5). Because a better understanding of the elusive phenomena of solid formation can enable powerful control of the processes involved, we direct further attention to the key factors controlling the nucleation and growth of nanoparticles in complicated environments (Section 6). Finally, we present outstanding questions and future opportunities (Section 7).

2. Advanced experimental techniques for detecting evolving nanoparticles

Recent advances in real-time and nanoscale analytical techniques allow us to capture the dynamic nucleation and growth processes of nanoparticles (15). Previously, to observe these processes on long time scales (> minutes) (16), researchers have made changes in the aqueous chemistry (e.g., pH and precursor concentrations (17) and used optical microscopies (18), and *ex situ* electron microscopies (19). However, these approaches have suffered from low resolution, low detection limits, and sample phase changes during the sample preparation or measurement. To address these limitations and to accurately reveal the fast dynamics of the nucleation and growth process of nanoparticles, the following new techniques have been utilized (Figure 1). Please note that this list is not meant to be definitive.

2.1. Liquid phase/cryogenic transmission electron microscopy (TEM)

Advanced TEM techniques, such as liquid phase TEM (LP-TEM) and cryogenic (cryo-TEM), greatly contribute to a deeper understanding of the dynamics of nanoparticles during their nucleation and growth. LP-TEM captures the evolution of nanoparticles in a liquid medium in a microfabricated cell with two Si₃N₄ windows separated by a 10–500 nm spacer (20). Cryo-TEM provides 3D structures of samples within a thin vitrified film of solution where all the components have been frozen by plunge-freezing in a coolant (21). Using these specialized microscopies, recent studies have revealed the presence of intermediate clusters during nucleation and have captured the movement of nanosized precursors during growth. For example, with a dual inlet LP-TEM stage, two formation pathways were found in supersaturated CaCO₃ solution: (i) crystalline phase formation with the consumption of the amorphous phase (Figure 1A-C) and (ii) direct formation of crystalline phases without a precursor phase (Figure 1D-F) (22). Cryo-TEM successfully revealed that poly(aspartic acid) strongly interacted with amorphous calcium carbonate (ACC) to cause its aggregation (Figure 1G-H) (23). These advanced TEM techniques have provided a clearer picture of the multiple-step processes of solid nucleation and growth in its early stage.

2.2. Fluid cell atomic force microscopy (AFM)

Fluid cell AFM provides real-time observations of surface morphological evolution in solution. Solutions are introduced into a fluid cell by a syringe drive at a constant flow rate (Figure 1I), and effluent from the fluid cell is collected by a fraction collector and analyzed (24). Fluid cell AFM can probe the dissolution of pre-existing surfaces (24), the nucleation of new nanoparticles (the particle density evolution) (25), particle growth (spiral/two-dimensional nucleation growth mode and step advance) (26), and their coupled processes (24). For example, Jun et al. examined

manganese carbonate dissolution and the subsequent oriented growth of manganese oxide on the manganese carbonate substrate by *in situ* AFM (Figure 1J) (24). *In situ* AFM measurements can also quantify nucleation rates (27), critical step lengths, and step formation energy (28; 29). Recently, an oriented face-specific nanocrystal probe of AFM was used to investigate the direction-specific interaction forces between nanocrystals (Figure 1K) (30).

2.3. X-ray scattering

Offering high sensitivity and improved statistics, synchrotron-based X-ray scattering techniques have been used extensively to identify the sizes and phases of nanoparticles. The small-angle X-ray scattering (SAXS) technique enables a statistically improved quantification of nanoparticles' size and shape and their aggregation and arrangement (Figure 1L-M) (31). In comparison, wide-angle X-ray scattering (WAXS) analyzes scattered electrons at larger angles, determining the crystallinity and phase of samples (32). In grazing incidence small/wide-angle X-ray scattering (GISAXS/GIWAXS), an X-ray beam is directed toward the sample surface at a grazing angle (α_i) that is close to, but smaller than, the critical angle (α_c) of the substrate. This operating geometry elongates the X-ray path length through the sample, providing up to 1000 times higher scattering intensity from nanoparticles formed on the substrate (Figure 1N-O) (31; 33; 34). In particular, GISAXS is highly effective in determining the size and shape of nanoparticles at interfaces (33; 35), and GIWAXS can detect the crystallinities and chemical phases of newly formed nanoparticles on surfaces (36; 37).

3. Classical and non-classical nucleation theory

3.1. Classical nucleation theory (CNT)

Classical nucleation theory (CNT) provides a good framework for explaining solid nucleation. The mathematical foundation for CNT was derived by Gibbs in the 1870s (38) and further developed by Volmer and Weber (39), Farkas (40), Becker and Döring (41), and Zeldovich (42). In CNT, a nucleus is regarded as a sphere with a surface tension equal to a theoretical flat interface (a capillarity approximation) and is assumed to be stable once formed (43). Quantitatively, the free energy of nucleation (ΔG) can be expressed as the sum of the bulk free energy and the surface free energy (Eq. (1)). At the critical nucleus size, the free energy of nucleation (ΔG) reaches its maximum (solid line in Figure 2A), where the free energy is called the nucleation energy barrier (ΔG^*). After overcoming ΔG^* , nuclei are stabilized and start to grow (Figure 2A and 2B). Hence, ΔG^* can control the nucleation rate (J), as expressed in Eq. (2). Depending on whether a foreign substrate is present, nucleation can be divided into homogenous nucleation (nucleation in solution) (44) and heterogeneous nucleation (nucleation on a substrate) (45).

$$\Delta G = -\frac{4}{3}\pi r^3 \left(\frac{\Delta\mu}{\nu_m}\right) + 4\pi r^2 \alpha \tag{1}$$

$$J = J_0 e^{\left(-\frac{\Delta G^*}{k_B T}\right)} = A e^{\left(-\frac{E_a}{k_B T}\right)} e^{\left(-\frac{\Delta G^*}{k_B T}\right)} \quad \text{where } \Delta G^* = \frac{16\pi v_m^2 (\alpha \text{ or } \alpha')^3}{3k_B^2 T^2 \sigma^2},$$
 (2)

where r is the radius of the nuclei, and $\Delta\mu$ is the chemical potential (= $k_BT\sigma$; saturation, σ = $\ln(IAP/K_{sp})$). IAP is the ion activity product and K_{sp} is the solubility product, v_m is the molecular volume of the nucleated phase (cm³·molecule⁻¹), α is the interfacial energy for homogeneous nucleation (mJ·m⁻²), α ' is the effective interfacial energy for heterogeneous nucleation (mJ·m⁻²), J_0 is a kinetic factor related to ion diffusion and nuclei surface properties, A is a pre-exponential kinetic factor related to ion diffusion and nuclei surface properties, and E_a is the apparent activation energy (J·mol⁻¹). k_B is the Boltzmann constant (1.38 × 10⁻²³ J·K⁻¹), and T is the temperature (K).

Recently, nanoscale advanced techniques have enabled a more comprehensive understanding of nucleation, especially its thermodynamic and kinetic aspects (α , J_0 , $\triangle G^*$, and E_a). Using Eq. (2), α (or α ') and J_0 can be calculated, respectively, from the slope and Y-intercept from a linear regression analysis of $\ln(J)$ versus $1/\sigma^2$. Utilizing the obtained α (or α '), ΔG^* can also be calculated. Here, the substrates' structure and surface properties can significantly affect α . With GISAXS, Li et al. quantified the α ' values of CaCO₃ nucleation on mica and quartz to be 24 mJ·m⁻² and 32 mJ·m⁻² for vaterite—mica and vaterite—quartz systems, respectively (3). The smaller α ' for vaterite-mica results from the smaller structural mismatch between CaCO₃ nuclei and mica than quartz. Hamm et al. also obtained α ' for calcite nucleation on different organic matrix functionalized substrates (46). Impurities in systems can also affect α ' (65). Zhu. et al. reported that a 0.9 mol% sulfate incorporation into CaCO₃ increased α by 11.7–15.4% (37). In addition to α ', the J_0 of CaCO₃ on quartz was measured to be $10^{16.1}$ nuclei·m⁻²·min⁻¹ at 25 °C (47). Wallace et al. reported the J_0 of silica nucleation ranges from $10^{13.5}$ to $10^{14.8}$ nuclei·m⁻²·min⁻¹ at room temperature (48). Moreover, by varying T, E_a can be determined from the slope of a linear regression of ln(J) versus 1/T (Figure 2C). The E_a values for CaCO₃ on quartz were reported to be 45 kJ·mol⁻¹ (47), and 32.8 kJ·mol⁻¹ for iron(III) (hydr)oxide nucleation on quartz (36). Such an accurate determination of these thermodynamic and kinetic parameters benefits the building of a holistic framework to precisely predict and control the nucleation process in the future.

3.2. Non-classical nucleation theory (N-CNT)

The spherical assumption of CNT may not be applicable when the nuclei contain fewer than 100 molecules (49), and CNT does not provide information about aggregate structures or pathways from solution to solid crystal (50). As an alternative, N-CNT was introduced to illustrate the

multiple intermediate metastable stages (e.g., prenucleation clusters, or PNCs) of nucleation that can occur preceding a thermodynamically stable phase (Figure 2A, dashed line) (51). Both experimental and computational efforts have been made to provide evidence to support N-CNT. Experimentally, nanometer-sized PNCs were found by titration experiments of dilute calcium chloride solution, which found a concentration difference between the measured calcium ions' concentration and the dosed calcium ions' concentration (Figure 2D) (52). The presence of PNCs with an ~2 nm diameter was further verified by analytical ultracentrifugation (AUC) of solutions drawn at different times in the prenucleation stage (52). Cryo-TEM also revealed the average diameters of PNCs to be 0.6–1.1 nm, smaller than that detected by AUC (53). Furthermore, electrospray ionization mass spectrometry (ESI-MS) has been utilized along with the X-ray absorption near edge structure (XANES) to show that highly hydrated networks are the PNCs for metal carbonates MCO₃ (M = Ca, Sr, Ba, Mn, Cd, and Pb) (54).

Modeling approaches such as molecular dynamics (MD) simulations have been utilized to examine the existence of PNCs. Using MD, Demichelis et al. proposed that PNCs are composed of dynamically ordered liquid-like oxyanion polymers (DOLLOP), including chains, branches, and rings (Figure 2E) (55), yet the stability of DOLLOPs has been questioned, because they can dissociate back into free ions and ion pairs (51). Using MD, Wallace et al. suggested that clusters are droplets of a dense liquid phase of CaCO₃·nH₂O that have formed by liquid–liquid separation (56). For calcium phosphate, using *ab initio* MD, it was found that calcium triphosphate PNC is more thermodynamically stable than free ions (57). Yang et al. demonstrated that ion association occurs between ions with the same charge and leads to calcium phosphate PNC formation *via* the consecutive coordination of the phosphate ions to calcium (58). Owing to the critical roles of the

PNCs in understanding and controlling solid nucleation and their phase and shape evolution, examining prenucleation stages of solid formation are currently an active research area.

3.3. Relationship between classical and non-classical nucleation

As discussed above, CNT offers a quantitative description of nucleation but does not describe the presence of intermediate stages. On the other hand, N-CNT describes multiple stages and the presence of amorphous/dense liquid/metastable phases but does not provide a quantitative description of the nucleation. To more accurately describe nucleation, it is important to connect the two theories. For example, Habraken et al. examined calcium phosphate formation and found amorphous calcium phosphate (ACP) formation, but the ACP formation could not be directly reconciled with CNT. Hence, to connect CNT and N-CNT, they introduced an 'excess free energy (ΔG_{Ex})' term, describing the impact of the PNCs on the free energy of calcium phosphate formation, as shown in Eq. (3) (59):

$$\Delta G_{N-CNT} = -\frac{4\pi f r^3}{3v_m} k_B T \sigma' + 4\pi f r^2 \alpha(r) - N \Delta G_{EX}, \qquad (3)$$

where ΔG_{N-CNT} is the free energy of nucleation when calcium phosphate PNCs are considered; f is a geometric factor that depends on the nucleus shape, taking values of 1 and 1/2 for spherical and hemispherical nuclei, respectively; σ' is supersaturation when considering PNCs, which equals $ln(IAP/K_{SP})^{1/\nu}$, where ν is the number of growth units in the material; $\alpha(r)$ is the interfacial energy of the nuclei; and N is the number of PNCs that combine to form the particle. ΔG_{Ex} , which expresses the interfacial energy of PNCs, decreases when clusters aggregate, resulting in a lower energy barrier of calcium phosphate nucleation (Figure 2F). Including ΔG_{Ex} in the energy consideration helps to explain how ACP nucleates first instead of the most thermodynamically stable phase, hydroxyapatite. Similarly, the decrease in the energy barrier of calcite nucleation on

carboxyl-terminated self-assembled monolayers has been estimated (60). Unfortunately, however, no experimental or modeling work has directly determined a value of ΔG_{Ex} , which calls for future systematic examination.

4. Classical and non-classical growth theories

4.1 Classical crystal growth

4.1.1 Classical crystal growth theory and new experimental findings

In the classical view, crystal growth is an atomic process in which monomeric growth units attach to pre-existing mineral surfaces and develop faceted crystals (61). Aqueous species, including ions, molecules, and atoms, are the primary constituents that incorporate into the crystal lattice. The overall growth rate (R) is related to σ as shown by Eq. (4):

$$R = k_a(\sigma - 1)^g \,, \tag{4}$$

where k_g is the growth rate constant, which is dependent on the solubility of the materials and temperature, and g is the growth order, signifying the growth mechanism. At relatively low σ , spiral growth (Figure 3A top) dominates the system, and the value of g is 2, resulting in a parabolic growth law (61). When σ is increased, two-dimensional (2D) nucleation dominates the system (Figure 3A, bottom). The growth rate changes exponentially change and g takes on values larger than 2 (61). Finally, as σ increases further, the surface becomes rough, growth is dominated by mass transfer, and g is equal to 1 (61).

Although the classical model has been successfully applied to understanding crystallization processes for many systems (62), it has also continuously evolved. Notably, with the advent of advanced techniques, more factors (e.g., kink densities, kink site specificities, and ion-pairs) have been added to classical growth theory to more precisely predict crystal growth. In the classical

theory, kinks are critical for incorporating new atoms into the surface, because incoming atoms at kink can immediately bond with more neighboring atoms than atoms on terraces and flat steps can (61). Therefore, the growth rate of a crystal, which is equivalent to the rate of molecule attachment to a pre-existing crystal, is closely related to the kink density of the surface at a fixed solute concentration. While a high kink density is assumed in the classical view (25), Zhang and Nancollas point out that, for sparingly soluble crystals at low temperatures, the equilibrium kink density should be low, and thus kink formation is an important contributor to controlling the kinetics of step-growth (63). Under this circumstance, kinks can be generated by one-dimensional (1D) nucleation. Previously, a kinetic Monte Carlo simulation was used to describe this process (64). As shown in Figure 3B, a solute molecule (orange circle) attaches to a fully occupied region of the step and creates a 1D nucleation (green circle), providing two new kink sites where further growth proceeds. Based on this principle, Joswiak et al. derived a supersaturation-dependent kink density expression (65).

Although the rates of attachment and detachment of precursors to kink sites are critical in determining the step advancement rate in growth, site specificities are often ignored. Stack et al. found that calcium-to-carbonate ratios can significantly change the growth patterns of calcite and that the attachment and detachment of aqueous calcium and carbonate ions should be treated separately (66). Therefore, for a crystal whose chemical formula is AB, we should separately consider the probability of ions A interacting with kinks and the probability of ions B interacting with kinks. Furthermore, recognizing the important roles of ion-pairs as metastable phases in N-CNT, recent studies have incorporated the role of ion-pairs in the crystal growth (67), as shown in Eq. (5):

$$R = 0.32 \cdot \frac{K_{AB,n}[A]^n [B]^n}{(1 + K_A[A])^n (1 + K_A[B])^n} \frac{k_B T}{h} e^{-\frac{\Delta G_{IP}}{RT}}.$$
 (5)

Here, n represents the number of ion-pairs in the attaching unit, $K_{AB,n}$ is the equilibrium constant for $[AB]_n$ complex formation in solution, h is Planck's constant, and ΔG_{IP} represents a reaction barrier for the ion-pairs formation.

4.2 Non-classical crystal growth

4.2.1 Oriented attachment and its kinetic models

Crystal growth can occur via the aggregation of nanosized crystals to form micron-sized crystals, which is called oriented attachment (OA) (68; 69). As shown in Figure 3C, OA has three steps: (i) self-assembly of primary nanocrystals (approaching), (ii) crystallographic reorganization within the self-assemblies (rotation), and (iii) conversion to oriented aggregates (contact) (62). By harnessing OA to control the facet selectivity of materials, material scientists can design crystalline structures with very specific geometries in one-, two-, or three-dimensions, and even create dislocations in the resulting crystal by promoting non-perfect attachment (68; 69). In this way, an improved understanding of the OA mechanism can shed light on the formation of anisotropic nanostructures and the evolution of their structural defects.

To decipher the OA process, colloidal aggregative behavior has been studied. To simulate the mono-dispersity of final particle sizes, early attempts at kinetic modeling had to assume that aggregation took place only between nuclei and large particles (70; 71). Eventually, this assumption was contradicted in later observations of single-single particle aggregation in LP-TEM measurements (72). To resolve this question, Huang, Zhang, and Banfield studied the growth of ZnS nanocrystals in the presence of mercaptoethanol and developed a model based on nanoparticle collisions (73). The evolution of the mean diameter (d) was described in Eq. (6), where d_{θ} is the mean diameter at t = 0 and k_{I} is the rate constant for oriented particle attachment:

$$d = \frac{d_0(\sqrt[3]{2}k_1t + 1)}{k_1t + 1}. (6)$$

Then, Zhang et al., further developed a multistep kinetic model based on the Smoluchowski equation, simulating the OA process with nanoparticles of varying sizes (74). To quantitatively describe the oriented-aggregation growth of zeolite, Tsapatsis and co-workers used the coalescence rate constant calculated from the Derjaguin–Landau–Verwey–Overbeek (DLVO) theory (75). A more recent work by Woehl and Prozorov found that the mobility of gold nanoparticles can determine whether OA happens through monomer–chain attachments or chain–chain attachments (76). The second-order aggregation kinetics revealed that the self-assembly rate increased approximately linearly with the nanoparticle diffusion coefficient.

4.2.2 Energy associated with OA and new experimental findings

A longstanding question regarding the OA process is what driving forces enable particles to achieve crystallographic coalignment and promote attachment-based growth. With new experimental methods, significant progress has been achieved in identifying the strength and range of the driving forces, including macroscopic interparticle interactions and interfacial water-induced interactions. Within the former, face-specific Van der Waals forces (vdW) were found to insignificantly affect azimuthal alignment at particle distances of 1.0–1.5 nm, but they are critical when particle distances are only one hydration layer thick (77). Nevertheless, another study investigating mica-mica adhesion showed that electrostatic interactions are the driving force for OA at short ranges and that vdW dominates at larger particle separations (78). Interfacial water structuring also contributed to the OA process. For example, dynamic force spectroscopy using nanoengineered single crystal probes showed that an attractive force between ZnO (0001) and ZnO(0001) with 60° rotational periodicity, and oriented attachment was water-mediated (Figure

3D) (30). Furthermore, macroscopic interparticle interactions and interfacial water-induced interactions can collaboratively control the OA process. Liu et al. illustrated that OA is driven by forces and torques arising from a combination of electrostatic ion-solvent correlations and dipolar interactions, even before the particles are within 5 nm (79).

5. Solid solution and phase transformation

Nucleation and growth are determined by two controlling energy factors (80): the free energy barrier (thermodynamics) and thermal energy (kinetics). These processes minimize the surface free energy in local space, making kinetically but less thermodynamically favored metastable phases form first, followed by their phase transformation to more thermodynamically favored structures. For example, ACC and ACP often appear first during nucleation (81; 82) and then transform to more crystalline phases.

In addition to thermodynamic and kinetic energy factors, differences in the bonding geometry of amorphous particles influence the pathway of phase transformation. For instance, ACP formed at a low Ca/P ratio mainly has monodentate bonding and directly transforms to hydroxyapatite. In contrast, ACP formed at a high Ca/P ratio mainly has bidentate bonding, and transforms to brushite first, and then to the most thermodynamically stable form, hydroxyapatite (82). These findings indicate that the ratios of building units alter the bonding structures in amorphous particles, and subsequently affect the pathways of phase transformation.

A solid solution is a mixture at the atomic level of at least two different solids that coexist as a new solid. Minor components are uniformly distributed in the crystal lattice of the major crystal structure. Some of the most studied solid solutions are calcium-magnesium-carbonate systems. At low Mg^{2+} activity (1.59 × 10⁻⁴), Mg^{2+} incorporates into the calcite lattice and enhances

the solubility of Mg-bearing calcite, decreasing the effective supersaturation needed for the calcites' growth (83). In another work, the metastability of ACC and amorphous magnesium carbonate (AMC) was altered by changing the Mg/(Ca+Mg) ratio (84). Furthermore, ACC's structure and its transformation pathway are also largely influenced by the addition of Mg. A recent study reported a new hydrated crystalline phase of CaCO₃ in the presence of Mg²⁺ (85): at an Mg/Ca molar ratio of 4.3~6.1, CaCO₃ hemihydrates with a needle-like crystal structure formed, which had not been observed previously. Here Mg²⁺ ions in the solution slowed the crystallization of the hydrated crystalline phase of CaCO₃ to monohydrated calcite. These findings proved the importance of Mg incorporation into CaCO₃ particles in determining the growth of CaCO₃, its phase transformation, and its structure.

6. Factors affecting nanoparticle nucleation and growth

6.1. Defects and facets

Substrate defects, such as steps and point defects, change the binding and adsorption energy between the precursor species and the substrate, altering the nucleation and growth of nanoparticles. Using LP-TEM, Zhu et al. explored the selective oxidation of Ag nanocrystals at different planar defects, such as nano twins and staking-faults (Figure 4A) (86). Ag₂O embryos preferentially nucleated at twinned tips and stacking faults, and they grew inward along the planar defects. However, the oxidation of metal was not observed away from the twinned tip of the facet (87), suggesting that Ag₂O selectively nucleated and grew at defects.

In particular, the surface energy at facets determines the growth rate of nanoparticles, and the nanoparticles grow to minimize their own surface energy. A low-energy facet exhibits a relatively slow growth rate, while a high-energy facet has a fast-growth rate, enabling it to have a

lower nanoparticle surface energy. As representative examples, nanoparticles' shapes were controlled by modifying the surface energy of the facet with surfactant adsorption, adjusting the facet's growth rate (88; 89). However, facet growth rates are determined by their surface energy only if nanoparticles are bigger than the critical size of nanoparticles. In a study of the dynamic growth of Pt nanocubes (90), when the nanoparticles were smaller than their critical particle size (~ 5 nm) for facet growth (up to 70 s in Figure 4B), ligands on the facets were easily removed, providing space for Pt growth. This process causes similar growth rates regardless of the facets' surface energy. After 70 s, when Pt nanoparticles grew bigger than their critical size, the growth rates of Pt nanoparticles at {111} facets were the highest, followed by those at {001} and {100} facets, indicating facet-dependent growth.

6.2. Heterogeneity of surfaces

In nature and engineering, the mineralogy and morphologies of substrate surfaces are heterogeneous, governed by their formation process and surrounding chemistry (91). Heterogeneous nucleation and growth are strongly connected with interfacial free energy, and thus accounting for the surface heterogeneity is crucial to understanding these processes.

Heterogeneous nucleation and growth are largely influenced by the following substrate's properties: its surface charge, interfacial energy, and surface morphology, and the lattice similarity between the precipitate and substrate (3; 92; 93). Hu et al. examined the heterogeneous nucleation and growth of iron(III) hydroxide on naturally abundant mineral substrates: quartz, muscovite, and corundum (Figure 4C) (92). They found that the heterogeneous nucleation rate of iron(III) (hydr)oxide minerals was faster on corundum than on other substrates. This fast nucleation was explained by a higher liquid–substrate interfacial energy (α_{ls}), confirmed by the water contact angle, and a lower substrate–nucleation interfacial energy (α_{sn}) from lattice similarity. In contrast, the

heterogeneous growth of iron(III) (hydr)oxide on corundum was rather slower than on quartz and mica. The positively charged iron(III) (hydr)oxide embryos were electrostatically repelled from the positively charged corundum, hindering their heterogeneous growth.

Both the surface morphology and the exposed substrate facets/planes deserve consideration in nucleation and growth. Unlike the effects of facets on nanoparticle growth discussed in **Section 6.1**, here, we discuss how the existing substrate facets/planes influence the heterogeneous nucleation and growth of minerals. Recently, Liu et al. demonstrated how manganese oxides were facet-selectively nucleated and grown on nanohematite (94). The selective nucleation of manganese oxides occurred owing to the surface oxygen coordination and bulk electron transfer mechanism. Then manganese oxides grew along the specific direction that minimized lattice mismatch, consequently forming manganese oxides nanowires on nanohematite. Even on the same mineral substrate, the shape and structure of heterogeneously formed manganese oxides were governed by the facet of the substrate, highlighting the importance of substrate facets on the nucleation and the growth of manganese oxides.

6.3. Electronic structure

The ubiquitous interactions between water and surfaces are centrally important in many disciplines, such as electrochemistry, materials science, and geology, (95-99). Because of the surface charge created by breaking hydrogen bonds at a surface, water molecules behave differently near the interface. Particularly, the surface charge at a solid—water interface induces an electrostatic field and consequently influences the alignment of cations, anions, and water molecules, creating an electric double layer (EDL). Because the EDL can alter reaction conditions kinetically and thermodynamically, the structure of the EDL is fundamental in the study of nanoparticle nucleation and growth. Recent studies have discussed inhomogeneous structures in the EDL resulting from

ion-ion correlations (Figure 4D) (100; 101). Interfacial surface charges occur as either homogeneously distributed charge densities or localized charge densities at discrete sites, depending on the identity of the cations (97; 101). The type of charge distribution affects the net orientation of water and the pH of a solution at the interface (95; 98; 100-102). As an example, using *in situ* high-resolution X-ray reflectivity, Lee et al. confirmed that the substantial enhancement of inner sphere complexed Rb⁺ near negatively charged mica far exceeds the amount needed for charge compensation of the mica surface (charge overscreening) (103). Hence, a full recognition of the effect of inhomogeneous structures in the EDL is crucial in understanding how materials form owing to differences in the concentrations of ions (95; 100; 101) and pH (100; 102), subsequently altering the saturation of the solution at the solid—water interface (25). In addition, the perturbation of local water structure by ions may also facilitate transport and decrease the energy barrier to the attachment of ions to the interfaces (104). In turn, newly formed particles can generate different surface potentials and add surface heterogeneities for subsequent reactions (105).

6.4. Water and ions at interfaces

Multiple interactions among the solvent, the foreign substrate, and ions can mediate the nucleation and growth of solids. In solid nucleation, the transformation from ionic clusters to a dense liquid phase is closely related to liquid–liquid separation (56). Moreover, the stability and dynamic behaviors of PNCs are strongly influenced by the water molecules (54). For example, aggregation of the PNCs was accompanied by a reduction of the mobility of water (55). In CNT, ion desolvation can determine E_a and J. In solid growth, the approach of an ion to the surface requires desolvation of both the surface and the ion, leading to a rate-limiting process for such 2-D nucleation (25). A metadynamic simulation demonstrated that the rate-limiting reaction for attachment in barite growth is a conversion of the inner-sphere adsorbed species to the bidentate

species (Figure 4D) (104). The desolvation effect is also a primary contributor to isotopic fractionation during CaCO₃ precipitation (106). In the case of ion—ion interactions, stable ion pairs at the nucleation stage have been considered as PNCs (52). At the growth stage, ion-pairs can also serve as precursors for growth (67).

6.5. Biological contributions

Mineral nucleation and growth induced by microorganisms are important in understanding geological elemental cycling and the rules that govern life. There are two fundamental mechanisms for bacterially-induced mineral nucleation:

(i) Passive nucleation, which occurs when the solution chemistry around bacteria cells is changed by microbial activities, such as bacterial ammonification, sulfate reduction in anoxic environments, and alkalization by cyanobacteria (107). These microbial activities release of CO₃²⁻ or HCO₃⁻ from bacteria or increase the solution pH, driving minerals to nucleate and grow. (ii) Active nucleation, which happens when bacteria cell surfaces contribute as nucleation sites (108). Owing to their small size (~2 μm³), large surface-to-volume ratio, and negative surface charge, bacteria are highly efficient at adsorbing metal cations from surrounding environments and concentrating them on their surfaces. Nucleation starts when these adsorbed cations interact with anions from the external milieu, driving the nucleation of (oxy)(hydr)oxides (109), carbonates (110), sulfates (111), sulfides (112), and phosphates (113).

In addition, soluble organic molecules or dissolved organic matter (DOM) contain high numbers of metal-binding sites, including carboxylates, phenols, amines, and thiols. Similar to microorganisms, the metal-ligand complexation of DOM alters the interactions between metal ions and aqueous anion counterparts. DOM has been shown to affect the nucleation of calcium

carbonates (114), iron oxyhydroxides (115), calcium sulfate (116), metal sulfides (117), and calcium phosphate (118). DOM affects the nucleation and growth of minerals through two mechanisms. First, DOM complexes with dissolved metal ions, decreasing the mineral saturation and the driving force for nucleation and growth (119; 120). Second, DOM adsorbs onto the surface of newly formed nanoclusters, further blocking the active growth sites for incoming new phases from the solution (115). Some organic polymers (e.g., poly(sodium 4-styrene sulfate)) can also affect the nucleation of minerals *via* binding with precursors (90).

6.6. Nanoconfinement

The nucleation and growth of particles in nanoscale porous media are critical in geological processes (121), biological processes (122), and engineering applications, such as the production of biopharmaceuticals (123) and semiconductors (124), and in water treatment (125). In confined nanopore spaces, the physicochemical properties of particles (e.g., thermotropism or polymorphism) are distinct from those in unconfined spaces (126; 127). The structure, dynamics, and thermodynamics of water in nanoconfinement can also affect the solvation free energies of ions and clusters (128; 129), altering nucleation and growth in nanopores. For a confined space, the Gibbs–Thomson equation describes the melting point depression ($\Delta T_{\rm m}$) of materials relative to the bulk form ($T_{\rm m,bulk}$) (126). Recently, Jin and Coasne reported a simulation study providing a molecular-level understanding of how nanoscale confinement shifts the melting point to a lower temperature (i.e., a decreased metastability barrier upon methane hydrate formation), which was previously observed experimentally and interpreted by the Gibbs-Thompson equation (130). On the other hand, for particles strongly adhered to the wall ($\theta < 90^{\circ}$), the melting point may increase in the confined space.

Nanoconfinement has been considered an essential aspect of biomineralization. For example, Cantaert et al. showed that 25–300 nm pores induced the formation of polycrystalline hydroxyapatite rod crystals via an intermediate ACP phase (131). Kim et al. suggested that modification of CNT is required to understand intrafibrillar collagen mineralization (i.e., mineralization inside collagen gap regions) (132). Owing to the nanoconfinement in the gap region (40 nm long and ~2 nm high) (133), calcium phosphate mineral is forced to nucleate and grow only in a lateral dimension (Figure 4E.1 and E.2). The 2D growth changes the relationship between nucleation rates (J) and supersaturation (σ) from $\ln(J) \propto 1/\sigma^2$ (for homogeneous nucleation of a sphere) to $\ln(J) \propto 1/\sigma$, explaining how confinement reduces the energy barrier to nucleation (Figure 4E.3). In bone mineralization, the extent of calcium phosphate formation inside the collagen gap region is closely related to mechanical properties such as the elastic modulus of tissue-level collagen matrices (134). Future research can harness the improved understanding of nucleation and growth in nanoconfinement for designing and developing stronger materials.

7. Outstanding questions and future opportunities

In recent decades, theoretical and experimental studies have elaborated the formation processes of nanoparticles, providing critical molecular insights into their behaviors and presenting new capabilities for controlling them (Figure 5). In this Section, we discuss outstanding questions and future opportunities for research and engineering in nucleation and growth.

7.1. Developing a holistic model to quantitatively describe nucleation and growth

A holistic quantitative description of nucleation and growth remains a great challenge. Here, we share our perspectives on building as a more complete quantitative model, one which unites classical and non-classical nucleation and growth behaviors. In the non-classical nucleation

process, PNCs, including disordered clusters and partially ordered agglomerates of clusters, aggregate and undergo a size-induced phase transition. Although several experimental and modeling studies have explored non-classical nucleation pathways, there is not yet a good quantitative N-CNT model for understanding the mechanisms of these processes and evaluating the kinetics involved. To the best of the authors' knowledge, there has been only a limited attempt to apply N-CNT in a quantitative description, specifically, by introducing 'excess free energy', as discussed in **Section 3.3** (59). However, this term captures only net effects, and it is still difficult to experimentally quantify the multiple intermediate steps. On the other hand, although PNCs and nanoparticles are different, studying the kinetics of nanoparticle OA can still provide insights into building a model for non-classical nucleation, because both CNT and N-CNT describe the aggregative behavior. For example, the kinetics model based on the Smoluchowski equation can also be applied to N-CNT (74) by considering the significant contributions of ion–solvent interactions within the PNCs to the cluster agglomeration/aggregation.

Although a holistic quantitative model that connects nucleation and growth would be ideal, for complicated systems that couple nucleation, growth, and phase transformation, developing such a comprehensive quantitative model is daunting. A good example is mesocrystal formation. In a recent *in situ* LP-TEM study, using aggregates of ferrihydrite as precursors, Zhu et al. found that oxalate can promote spindle-shaped hematite mesocrystal formation, while in the absence of oxalate, segregated hematite nanoparticles formed (135). Here, dissolution of ferrihydrite provided the precursors for hematite nucleation. Importantly, the interfacial gradients of Fe³⁺ concentration at the oxalate-covered hematite surface induced new hematite nucleation adjacent to the primary hematite nanoparticles. Then, attractive particle interactions drove OA of nanoparticles to form the hematite mesocrystal. In this case, the convoluted processes of old precursor phase dissolution,

new phase nucleation, and OA made the development of a quantitative description extremely difficult. To overcome this challenge, artificial intelligence technology, specifically machine learning (ML), can be an effective tool for determining and predicting multiple parameter optimization. ML has been successful in describing the physical and chemical thresholds for defining clusters, nanoparticles, and bulk states of silver (136) and in predicting/optimizing the synthetic nucleation and growth of CdSe/CdS (137). Future nucleation and growth investigations with ML hold great promise for describing the relative contributions from multiple processes and ultimately providing a quantitative description of complicated systems.

7.2. Connecting experimental data and computational simulations

Molecular dynamics have been extended continuously, including *ab initio* MD. Density-functional theory (DFT), the dominant electronic structure method of *ab initio* MD, has become standard for describing/predicting the nucleation process (138). There have been many successful simulations for mineral nucleation, especially for the existence or formulation of PNCs for N-CNT. For example, the DFT model quantified how solutions with different Mg:Ca ratios affect the nucleation barriers of calcite and aragonite. The results demonstrate that the nucleation barrier of calcite exceeds that of aragonite in solutions with Mg:Ca ratios consistent with seawater (139). MD also proved that nanodroplets of dense liquid cluster coalesce and solidify into ACC (56). Further, the MD method has shown the existence of mineral clusters made of ionic polymers in the shape of chains, branches, and rings as PNCs (55).

However, computational studies that better connect with experimental nucleation and growth results are still needed. For example, small systems (10^2-10^4 particles) are often modeled under ideal conditions. Because the interfacial description requires more restricted and reliable force fields, predicting a realistic nucleation system is more complicated (43). Besides, simulation

results are specific to certain limited physical approximations in order to reduce the complexity of the potential. The results can be inflexible and provide only limited information on complex energy landscapes (140). Thus, future efforts should include the following:

- (i) To effectively determine energies and forces in large-scale simulations, we need more efficient potentials that can replace computationally extensive electronic structure calculations. For example, atomistic potentials describe the relationship between atomic configurations and potential energies. They use less sophisticated analytic functions of the atomic coordinates, which is helpful for fast evaluation of large-scale simulations (140).
- (ii) ML potentials can directly use or combine a variety of functions, capturing various types of bonding, such as covalent bonding (141). Because the ML potentials are more general forms that, unlike classical MD, are not based on physical considerations, they can increase the simulation scale and achieve an accuracy rate closer to that of first-principles calculations (142).

Acknowledgments

We are grateful for the support received from the U.S. National Science Foundation (CHE-1905077), the America Chemical Society's Petroleum Research Fund (62756-ND5), and the U.S. Environmental Protection Agency (EPA, Assistance Agreement No. 84008401). The review has not been formally reviewed by the EPA. The views expressed in this document are solely those of the authors of this article and do not necessarily reflect those of the Agency. The EPA does not endorse any products or commercial services mentioned in this publication. We wish to thank the members of the Environmental NanoChemistry Group for their valuable discussions. We thank Prof. James Ballard, Mr. Albern Tan, and Prof. Sandra Matteucci for their careful reviews of the manuscript.

References

- 1. Kulmala M, Kontkanen J, Junninen H, Lehtipalo K, Manninen HE, et al. 2013. Direct observations of atmospheric aerosol nucleation. *Science* 339:943-6
- Jung H, Lee B, Lengyel M, Axelbaum R, Yoo J, et al. 2018. Nanoscale In Situ Detection of Nucleation and Growth of Li Electrodeposition at Various Current Densities. *J. Mater.* Chem. A 6:4629-35
- 3. Li Q, Fernandez-Martinez A, Lee B, Waychunas GA, Jun Y-S. 2014. Interfacial Energies for Heterogeneous Nucleation of Calcium Carbonate on Mica and Quartz. *Environmental Science & Technology* 48:5745-53
- 4. Butterfield CN, Soldatova AV, Lee S-W, Spiro TG, Tebo BM. 2013. Mn (II, III) oxidation and MnO₂ mineralization by an expressed bacterial multicopper oxidase. *Proceedings of the National Academy of Sciences* 110:11731-5
- 5. Byrne JM, Klueglein N, Pearce C, Rosso KM, Appel E, Kappler A. 2015. Redox cycling of Fe (II) and Fe (III) in magnetite by Fe-metabolizing bacteria. *Science* 347:1473-6
- 6. Jung H, Taillefert M, Sun J, Wang Q, Borkiewicz OJ, et al. 2020. Redox Cycling Driven Transformation of Layered Manganese Oxides to Tunnel Structures. *J. Am. Chem. Soc.* 142:2506-13
- 7. Nudelman F, Pieterse K, George A, Bomans PHH, Friedrich H, et al. 2010. The role of collagen in bone apatite formation in the presence of hydroxyapatite nucleation inhibitors.

 Nat. Mater. 9:1004-9
- 8. Addadi L, Raz S, Weiner S. 2003. Taking advantage of disorder: amorphous calcium carbonate and its roles in biomineralization. *Advanced Materials* 15:959-70
- 9. Treat ND, Malik JAN, Reid O, Yu L, Shuttle CG, et al. 2013. Microstructure formation in molecular and polymer semiconductors assisted by nucleation agents. *Nature materials* 12:628-33
- Cleveland CL, Landman U, Schaaff TG, Shafigullin MN, Stephens PW, Whetten RL. 1997.
 Structural evolution of smaller gold nanocrystals: The truncated decahedral motif. *Physical review letters* 79:1873
- 11. Alivisatos AP. 1996. Semiconductor clusters, nanocrystals, and quantum dots. *Science* 271:933-7

- 12. Friedman G, Schultz D. 1994. Precipitation of vaterite (CaCO3) during oil field drilling.

 Mineralogical Magazine 58:401-8
- 13. Moghadasi J, Jamialahmadi M, Müller-Steinhagen H, Sharif A, Izadpanah M, et al. Formation damage in Iranian oil fields. *Proc. International Symposium and Exhibition on Formation Damage Control*, 2002: Society of Petroleum Engineers
- 14. Hochella MF, Lower SK, Maurice PA, Penn RL, Sahai N, et al. 2008. Nanominerals, mineral nanoparticles, and earth systems. *Science* 319:1631-5
- 15. Chen Q, Yuk JM, Hauwiller MR, Park J, Dae KS, et al. 2020. Nucleation, growth, and superlattice formation of nanocrystals observed in liquid cell transmission electron microscopy. *MRS Bulletin* 45:713-26
- 16. Zhang TH, Liu XY. 2014. Experimental modelling of single-particle dynamic processes in crystallization by controlled colloidal assembly. *Chemical Society Reviews* 43:2324-47
- 17. Lioliou MG, Paraskeva CA, Koutsoukos PG, Payatakes AC. 2007. Heterogeneous nucleation and growth of calcium carbonate on calcite and quartz. *Journal of Colloid and Interface Science* 308:421-8
- 18. Gasser U, Weeks ER, Schofield A, Pusey P, Weitz D. 2001. Real-space imaging of nucleation and growth in colloidal crystallization. *Science* 292:258-62
- 19. Barrere F, Snel MM, Van Blitterswijk CA, de Groot K, Layrolle P. 2004. Nano-scale study of the nucleation and growth of calcium phosphate coating on titanium implants. *Biomaterials* 25:2901-10
- 20. Yuk JM, Park J, Ercius P, Kim K, Hellebusch DJ, et al. 2012. High-resolution EM of colloidal nanocrystal growth using graphene liquid cells. *Science* 336:61-4
- 21. Nudelman F, Sommerdijk NA. 2011. Cryo-electron tomography: 3-dimensional imaging of soft matter. *Soft Matter* 7:17-24
- 22. Nielsen MH, Aloni S, De Yoreo JJ. 2014. In situ TEM imaging of CaCO₃ nucleation reveals coexistence of direct and indirect pathways. *Science* 345:1158-62
- 23. Xu Y, Tijssen KC, Bomans PH, Akiva A, Friedrich H, et al. 2018. Microscopic structure of the polymer-induced liquid precursor for calcium carbonate. *Nature communications* 9:1-12

- 24. Jun Y-S, Kendall TA, Martin ST, Friend CM, Vlassak JJ. 2005. Heteroepitaxial nucleation and oriented growth of manganese oxide islands on carbonate minerals under aqueous conditions. *Environmental science & technology* 39:1239-49
- 25. De Yoreo JJ, Vekilov PG. 2003. Principles of crystal nucleation and growth. *Reviews in mineralogy* 54:57-93
- 26. Ruiz-Agudo E, Putnis C. 2012. Direct observations of mineral fluid reactions using atomic force microscopy: the specific example of calcite. *Mineralogical Magazine* 76:227-53
- 27. Wang L, Ruiz-Agudo En, Putnis CV, Menneken M, Putnis A. 2012. Kinetics of calcium phosphate nucleation and growth on calcite: Implications for predicting the fate of dissolved phosphate species in alkaline soils. *Environmental science & technology* 46:834-42
- 28. Cao Y, Li M, Cheng M, Song J, Hu Z. 2014. An in situ AFM investigation on the morphology of the (100) growth interface of ZTS crystal. *Journal of Crystal Growth* 388:22-8
- 29. Teng HH, Dove PM, Orme CA, De Yoreo JJ. 1998. Thermodynamics of calcite growth: baseline for understanding biomineral formation. *Science* 282:724-7
- 30. Zhang X, Shen Z, Liu J, Kerisit S, Bowden M, et al. 2017. Direction-specific interaction forces underlying zinc oxide crystal growth by oriented attachment. *Nature communications* 8:1-8
- 31. Li T, Senesi AJ, Lee B. 2016. Small angle X-ray scattering for nanoparticle research. *Chemical reviews* 116:11128-80
- 32. Cammarata M, Levantino M, Schotte F, Anfinrud PA, Ewald F, et al. 2008. Tracking the structural dynamics of proteins in solution using time-resolved wide-angle X-ray scattering.

 Nature methods 5:881-6
- 33. Jun Y-S, Lee B, Waychunas GA. 2010. In situ observations of nanoparticle early development kinetics at mineral— water interfaces. *Environmental science technology* 44:8182-9
- 34. Levine JR, Cohen J, Chung Y, Georgopoulos P. 1989. Grazing-incidence small-angle X-ray scattering: new tool for studying thin film growth. *Journal of Applied Crystallography* 22:528-32

- 35. Rauscher M, Paniago R, Metzger H, Kovats Z, Domke J, et al. 1999. Grazing incidence small angle x-ray scattering from free-standing nanostructures. *Journal of Applied Physics* 86:6763-9
- 36. Wu X, Lee B, Jun Y-S. 2020. Interfacial and Activation Energies of Environmentally Abundant Heterogeneously Nucleated Iron (III)(Hydr) oxide on Quartz. *Environmental Science Technology* 54:12119-29
- 37. Zhu Y, Li Q, Kim D, Min Y, Lee B, Jun Y-S. 2021. Sulfate-Controlled Heterogeneous CaCO₃ Nucleation and Its Non-linear Interfacial Energy Evolution. *Environmental Science Technology*
- 38. Gibbs JW. 1879. On the equilibrium of heterogeneous substances.
- 39. Volmer M, Weber A. 1926. Germ-formation in oversaturated figures. *Z. phys. chem* 119:277-301
- 40. Farkas L. 1927. Nucleation Rates in Supersaturated Vapours. Z. Phys. Chem 125:236
- 41. Becker R, Döring W. 1935. Kinetische behandlung der keimbildung in übersättigten dämpfen. *Annalen der Physik* 416:719-52
- 42. Zeldovich YB. 1943. On the theory of new phase formation: cavitation. *Acta Physicochem.*, *USSR* 18:1
- 43. Sosso GC, Chen J, Cox SJ, Fitzner M, Pedevilla P, et al. 2016. Crystal nucleation in liquids: Open questions and future challenges in molecular dynamics simulations. *Chemical reviews* 116:7078-116
- 44. Wagner P, Strey R. 1984. Measurements of homogeneous nucleation rates for n-nonane vapor using a two-piston expansion chamber. *The Journal of chemical physics* 80:5266-75
- 45. Liu X. 2000. Heterogeneous nucleation or homogeneous nucleation? *The Journal of Chemical Physics* 112:9949-55
- 46. Hamm LM, Giuffre AJ, Han N, Tao J, Wang D, et al. 2014. Reconciling disparate views of template-directed nucleation through measurement of calcite nucleation kinetics and binding energies. *Proceedings of the National Academy of Sciences* 111:1304-9
- 47. Li Q, Jun Y-S. 2018. The apparent activation energy and pre-exponential kinetic factor for heterogeneous calcium carbonate nucleation on quartz. *Communications Chemistry* 1:1-9

- 48. Wallace AF, DeYoreo JJ, Dove PM. 2009. Kinetics of silica nucleation on carboxyl-and amine-terminated surfaces: insights for biomineralization. *Journal of the American Chemical Society* 131:5244-50
- 49. Yau S-T, Vekilov PG. 2000. Quasi-planar nucleus structure in apoferritin crystallization.

 Nature 406:494-7
- 50. Karthika S, Radhakrishnan T, Kalaichelvi P. 2016. A review of classical and nonclassical nucleation theories. *Crystal Growth & Design* 16:6663-81
- 51. Smeets PJ, Finney AR, Habraken WJ, Nudelman F, Friedrich H, et al. 2017. A classical view on nonclassical nucleation. *Proceedings of the National Academy of Sciences* 114:E7882-E90
- 52. Gebauer D, Völkel A, Cölfen H. 2008. Stable prenucleation calcium carbonate clusters. Science 322:1819-22
- 53. Pouget EM, Bomans PH, Goos JA, Frederik PM, Sommerdijk NA. 2009. The initial stages of template-controlled CaCO3 formation revealed by cryo-TEM. *Science* 323:1455-8
- 54. Wolf SE, Müller L, Barrea R, Kampf CJ, Leiterer J, et al. 2011. Carbonate-coordinated metal complexes precede the formation of liquid amorphous mineral emulsions of divalent metal carbonates. *Nanoscale* 3:1158-65
- 55. Demichelis R, Raiteri P, Gale JD, Quigley D, Gebauer D. 2011. Stable prenucleation mineral clusters are liquid-like ionic polymers. *Nature communications* 2:1-8
- 56. Wallace AF, Hedges LO, Fernandez-Martinez A, Raiteri P, Gale JD, et al. 2013. Microscopic evidence for liquid-liquid separation in supersaturated CaCO3 solutions. Science 341:885-9
- 57. Mancardi G, Terranova U, de Leeuw NH. 2016. Calcium phosphate prenucleation complexes in water by means of ab initio molecular dynamics simulations. *Crystal Growth & Design* 16:3353-8
- 58. Yang X, Wang M, Yang Y, Cui B, Xu Z, Yang X. 2019. Physical origin underlying the prenucleation-cluster-mediated nonclassical nucleation pathways for calcium phosphate. *Physical Chemistry Chemical Physics* 21:14530-40

- 59. Habraken WJ, Tao J, Brylka LJ, Friedrich H, Bertinetti L, et al. 2013. Ion-association complexes unite classical and non-classical theories for the biomimetic nucleation of calcium phosphate. *Nature communications* 4:1-12
- 60. Hu Q, Nielsen MH, Freeman C, Hamm L, Tao J, et al. 2012. The thermodynamics of calcite nucleation at organic interfaces: Classical vs. non-classical pathways. *Faraday Discussions* 159:509-23
- 61. Chernov AA. 2012. *Modern crystallography III: crystal growth*. Springer Science & Business Media
- 62. Van Driessche AE, Kellermeier M, Benning LG, Gebauer D. 2016. New perspectives on mineral nucleation and growth: from solution precursors to solid materials. Springer
- 63. Zhang J, Nancollas GH. 1990. Kink densities along a crystal surface step at low temperatures and under nonequilibrium conditions. *Journal of crystal growth* 106:181-90
- 64. De Yoreo J, Zepeda-Ruiz L, Friddle R, Qiu S, Wasylenki L, et al. 2009. Rethinking classical crystal growth models through molecular scale insights: consequences of kink-limited kinetics. *Crystal Growth & Design* 9:5135-44
- 65. Joswiak MN, Peters B, Doherty MF. 2018. Nonequilibrium Kink Density from One-Dimensional Nucleation for Step Velocity Predictions. Crystal Growth & Design 18:723-7
- 66. Stack AG, Grantham MC. 2010. Growth rate of calcite steps as a function of aqueous calcium-to-carbonate ratio: independent attachment and detachment of calcium and carbonate ions. *Crystal Growth & Design* 10:1409-13
- 67. Andersson M, Dobberschütz S, Sand KK, Tobler D, De Yoreo JJ, Stipp S. 2016. A microkinetic model of calcite step growth. *Angewandte Chemie* 128:11252-6
- 68. Penn RL, Banfield JF. 1999. Morphology development and crystal growth in nanocrystalline aggregates under hydrothermal conditions: Insights from titania. *Geochimica et cosmochimica acta* 63:1549-57
- 69. Penn RL, Banfield JF. 1998. Imperfect oriented attachment: dislocation generation in defect-free nanocrystals. *Science* 281:969-71
- 70. Dirksen J, Benjelloun S, Ring T. 1990. Modelling the precipitation of copper oxalate aggregates. *Colloid and Polymer Science* 268:864-76

- 71. Park J, Privman V, Matijević E. 2001. Model of formation of monodispersed colloids. *The Journal of Physical Chemistry B* 105:11630-5
- 72. Zhu C, Liang S, Song E, Zhou Y, Wang W, et al. 2018. In-situ liquid cell transmission electron microscopy investigation on oriented attachment of gold nanoparticles. *Nature communications* 9:1-7
- 73. Huang F, Zhang H, Banfield JF. 2003. The role of oriented attachment crystal growth in hydrothermal coarsening of nanocrystalline ZnS. *The Journal of Physical Chemistry B* 107:10470-5
- 74. Zhang J, Lin Z, Lan Y, Ren G, Chen D, et al. 2006. A multistep oriented attachment kinetics: coarsening of ZnS nanoparticle in concentrated NaOH. *Journal of the American Chemical Society* 128:12981-7
- 75. Davis TM, Drews TO, Ramanan H, He C, Dong J, et al. 2006. Mechanistic principles of nanoparticle evolution to zeolite crystals. *Nature materials* 5:400-8
- 76. Woehl TJ, Prozorov T. 2015. The mechanisms for nanoparticle surface diffusion and chain self-assembly determined from real-time nanoscale kinetics in liquid. *The Journal of Physical Chemistry C* 119:21261-9
- 77. Hopkins JC, Podgornik R, Ching W-Y, French RH, Parsegian VA. 2015. Disentangling the effects of shape and dielectric response in van der Waals interactions between anisotropic bodies. *The Journal of Physical Chemistry C* 119:19083-94
- 78. Li D, Chun J, Xiao D, Zhou W, Cai H, et al. 2017. Trends in mica–mica adhesion reflect the influence of molecular details on long-range dispersion forces underlying aggregation and coalignment. *Proceedings of the National Academy of Sciences* 114:7537-42
- 79. Liu L, Nakouzi E, Sushko ML, Schenter GK, Mundy CJ, et al. 2020. Connecting energetics to dynamics in particle growth by oriented attachment using real-time observations. *Nature communications* 11:1-11
- 80. De Yoreo JJ, Gilbert PU, Sommerdijk NA, Penn RL, Whitelam S, et al. 2015. Crystallization By Particle Attachment in Synthetic, Biogenic, and Geologic Environments. *Science* 349

- 81. Liu Z, Zhang Z, Wang Z, Jin B, Li D, et al. 2020. Shape-Preserving Amorphous-to-Crystalline Transformation of CaCO₃ Revealed By In Situ TEM. *Proceedings of the National Academy of Sciences* 117:3397-404
- 82. Hoeher AJ, Mergelsberg ST, Borkiewicz OJ, Michel FM. 2021. Impacts of Initial Ca/P on Amorphous Calcium Phosphate. *Crystal Growth & Design*
- 83. Davis KJ, Dove PM, De Yoreo JJ. 2000. The Role of Mg²⁺ as An Impurity in Calcite Growth. *Science* 290:1134-7
- 84. Radha A, Fernandez-Martinez A, Hu Y, Jun Y-S, Waychunas GA, Navrotsky A. 2012. Energetic and Structural Studies of Amorphous Ca_{1− x}Mg_xCO₃· nH₂O (0≤ x≤ 1). Geochimica et Cosmochimica Acta 90:83-95
- 85. Zou Z, Habraken WJ, Matveeva G, Jensen AC, Bertinetti L, et al. 2019. A Hydrated Crystalline Calcium Carbonate Phase: Calcium Carbonate Hemihydrate. *Science* 363:396-400
- 86. Zhu Q, Pan Z, Zhao Z, Cao G, Luo L, et al. 2021. Defect-Driven Selective Metal Oxidation at Atomic Scale. *Nature Communications* 12:1-8
- 87. Burrows ND, Hale CR, Penn RL. 2012. Effect of ionic strength on the kinetics of crystal growth by oriented aggregation. *Crystal Growth & Design* 12:4787-97
- 88. Xiao J, Qi L. 2011. Surfactant-Assisted, Shape-Controlled Synthesis of Gold Nanocrystals.

 Nanoscale 3:1383-96
- 89. Jun Y-w, Casula MF, Sim J-H, Kim SY, Cheon J, Alivisatos AP. 2003. Surfactant-Assisted Elimination of A High energy Facet as A Means of Controlling The Shapes of TiO₂ Nanocrystals. *Journal of the American Chemical Society* 125:15981-5
- 90. Liao H-G, Zherebetskyy D, Xin H, Czarnik C, Ercius P, et al. 2014. Facet Development During Platinum Nanocube Growth. *Science* 345:916-9
- 91. Werner F, Mueller CW, Thieme J, Gianoncelli A, Rivard C, et al. 2017. Micro-Scale Heterogeneity of Soil Phosphorus Depends on Soil Substrate And Depth. *Scientific Reports* 7:1-9
- 92. Hu Y, Neil C, Lee B, Jun Y-S. 2013. Control of Heterogeneous Fe (III)(Hydr)oxide Nucleation and Growth by Interfacial Energies and Local Saturations. *Environmental Science & Technology* 47:9198-206

- 93. Ray JR, Lee B, Baltrusaitis J, Jun Y-S. 2012. Formation of Iron (III)(Hydr)oxides on Polyaspartate- and Alginate-Coated Substrates: Effects of Coating Hydrophilicity and Functional Group. *Environmental Science & Technology* 46:13167-75
- 94. Liu J, Inoué S, Zhu R, He H, Hochella Jr MF. 2021. Facet-Specific Oxidation of Mn (II) and Heterogeneous Growth of Manganese (Oxyhydr)oxides on Hematite Nanoparticles. *Geochimica et Cosmochimica Acta*
- 95. Elhadj S, De Yoreo JJ, Hoyer JR, Dove PM. 2006. Role of molecular charge and hydrophilicity in regulating the kinetics of crystal growth. 103:19237-42
- 96. Ohlin CA, Villa EM, Rustad JR, Casey WHJNm. 2010. Dissolution of insulating oxide materials at the molecular scale. 9:11-9
- 97. Gonella G, Backus EHG, Nagata Y, Bonthuis DJ, Loche P, et al. 2021. Water at charged interfaces. *Nature Reviews Chemistry* 5:466-85
- 98. Li L, Fijneman AJ, Kaandorp JA, Aizenberg J, Noorduin WL. 2018. Directed nucleation and growth by balancing local supersaturation and substrate/nucleus lattice mismatch. 115:3575-80
- 99. Aber JE, Arnold S, Garetz BA, Myerson ASJPrl. 2005. Strong dc electric field applied to supersaturated aqueous glycine solution induces nucleation of the γ polymorph. 94:145503
- 100. Gibbs-Davis JM, Kruk JJ, Konek CT, Scheidt KA, Geiger FMJJotACS. 2008. Jammed Acid- Base Reactions at Interfaces. 130:15444-7
- 101. Dewan S, Carnevale V, Bankura A, Eftekhari-Bafrooei A, Fiorin G, et al. 2014. Structure of Water at Charged Interfaces: A Molecular Dynamics Study. *Langmuir* 30:8056-65
- 102. Katsounaros I, Meier JC, Klemm SO, Topalov AA, Biedermann PU, et al. 2011. The effective surface pH during reactions at the solid–liquid interface. *Electrochemistry Communications* 13:634-7
- 103. Lee SS, Koishi A, Bourg IC, Fenter P. 2021. Ion correlations drive charge overscreening and heterogeneous nucleation at solid–aqueous electrolyte interfaces. *Proceedings of the National Academy of Sciences* 118:e2105154118
- 104. Stack AG, Raiteri P, Gale JD. 2012. Accurate rates of the complex mechanisms for growth and dissolution of minerals using a combination of rare-event theories. *Journal of the American Chemical Society* 134:11-4

- 105. Kendall TA, Na C, Jun YS, Martin ST. 2008. Electrical properties of mineral surfaces for increasing water sorption. *Langmuir* 24:2519-24
- 106. DePaolo DJ. 2011. Surface kinetic model for isotopic and trace element fractionation during precipitation of calcite from aqueous solutions. *Geochimica et cosmochimica acta* 75:1039-56
- 107. Stocks-Fischer S, Galinat JK, Bang SS. 1999. Microbiological precipitation of CaCO₃. *Soil Biology Biochemistry* 31:1563-71
- 108. Schultze-Lam S, Fortin D, Davis B, Beveridge T. 1996. Mineralization of bacterial surfaces.

 Chemical Geology 132:171-81
- 109. Anderson C, Pedersen K. 2003. In situ growth of Gallionella biofilms and partitioning of lanthanides and actinides between biological material and ferric oxyhydroxides. *Geobiology* 1:169-78
- 110. Rivadeneyra MA, Martín-Algarra A, Sánchez-Román M, Sánchez-Navas A, Martín-Ramos JD. 2010. Amorphous Ca-phosphate precursors for Ca-carbonate biominerals mediated by Chromohalobacter marismortui. *The ISME journal* 4:922-32
- 111. González-Muñoz MT, Rodriguez-Navarro C, Martínez-Ruiz F, Arias JM, Merroun ML, Rodriguez-Gallego M. 2010. Bacterial biomineralization: new insights from Myxococcus-induced mineral precipitation. *Geological Society, London, Special Publications* 336:31-50
- 112. Ferris F, Fyfe W, Beveridge T. 1987. Bacteria as nucleation sites for authigenic minerals in a metal-contaminated lake sediment. *Chemical Geology* 63:225-32
- 113. Frankel RB, Bazylinski DA. 2003. Biologically induced mineralization by bacteria.

 Reviews in mineralogy geochemistry 54:95-114
- 114. Chave KE. 1965. Carbonates: association with organic matter in surface seawater. *Science* 148:1723-4
- 115. Wu X, Bowers B, Kim D, Lee B, Jun Y-S. 2019. Dissolved organic matter affects arsenic mobility and iron (III)(hydr) oxide formation: implications for managed aquifer recharge. *Environmental science technology* 53:14357-67
- 116. Van Driessche A, Stawski T, Kellermeier M. 2019. Calcium sulfate precipitation pathways in natural and engineered environments. *Chemical Geology* 530:119274

- 117. Lau BL, Hsu-Kim H. 2008. Precipitation and growth of zinc sulfide nanoparticles in the presence of thiol-containing natural organic ligands. *Environmental science technology* 42:7236-41
- 118. Barati D, Walters JD, Pajoum Shariati SR, Moeinzadeh S, Jabbari E. 2015. Effect of organic acids on calcium phosphate nucleation and osteogenic differentiation of human mesenchymal stem cells on peptide functionalized nanofibers. *Langmuir* 31:5130-40
- 119. Chave KE, Suess E. 1970. Calcium Carbonate Saturation in Seawater: Effects of Dissolved Organic Matter. *Limnology Oceanography* 15:633-7
- 120. Rose AL, Waite TD. 2002. Kinetic model for Fe (II) oxidation in seawater in the absence and presence of natural organic matter. *Environmental Science Technology* 36:433-44
- 121. Wang Y. 2014. Nanogeochemistry: Nanostructures, emergent properties and their control on geochemical reactions and mass transfers. *Chem. Geol.* 378–379:1-23
- 122. Yang L, Killian CE, Kunz M, Tamura N, Gilbert PUPA. 2011. Biomineral nanoparticles are space-filling. *Nanoscale* 3:603-9
- 123. Artusio F, Pisano R. 2018. Surface-induced crystallization of pharmaceuticals and biopharmaceuticals: A review. *International journal of pharmaceutics* 547:190-208
- 124. Alaei A, Zong K, Asawa K, Chou T-M, Briseño AL, et al. 2021. Orienting and shaping organic semiconductor single crystals through selective nanoconfinement. *Soft Matter* 17:3603-8
- 125. Qian J, Gao X, Pan B. 2020. Nanoconfinement-mediated water treatment: From fundamental to application. *Environmental Science & Technology* 54:8509-26
- 126. Jiang Q, Ward MD. 2014. Crystallization under nanoscale confinement. *Chem. Soc. Rev.* 43:2066-79
- 127. Hamilton BD, Ha J-M, Hillmyer MA, Ward MD. 2012. Manipulating Crystal Growth and Polymorphism by Confinement in Nanoscale Crystallization Chambers. *Accounts of Chemical Research* 45:414-23
- 128. Fumagalli L, Esfandiar A, Fabregas R, Hu S, Ares P, et al. 2018. Anomalously low dielectric constant of confined water. *Science* 360:1339

- 129. Le Caër S, Pin S, Esnouf S, Raffy Q, Renault JP, et al. 2011. A trapped water network in nanoporous material: the role of interfaces. *Physical Chemistry Chemical Physics* 13:17658-66
- 130. Jin D, Coasne B. 2021. Reduced phase stability and faster formation/dissociation kinetics in confined methane hydrate. *Proceedings of the National Academy of Sciences* 118
- 131. Cantaert B, Beniash E, Meldrum FC. 2013. Nanoscale confinement controls the crystallization of calcium phosphate: relevance to bone formation. *Chem. Eur. J.* 19:14918-24
- 132. Kim D, Lee B, Thomopoulos S, Jun Y-S. 2018. The role of confined collagen geometry in decreasing nucleation energy barriers to intrafibrillar mineralization. *Nature Communications* 9:962
- 133. Alexander B, Daulton TL, Genin GM, Lipner J, Pasteris JD, et al. 2012. The nanometre-scale physiology of bone: steric modelling and scanning transmission electron microscopy of collagen–mineral structure. *J. R. Soc., Interface* 9:1774-86
- 134. Kim D, Lee B, Marshall BP, Thomopoulos S, Jun Y-S. 2021. Cyclic Strain Enhances the Early Stage Mineral Nucleation and the Modulus of Demineralized Bone Matrix. *Biomaterials Science*
- 135. Zhu G, Sushko ML, Loring JS, Legg BA, Song M, et al. 2021. Self-similar mesocrystals form via interface-driven nucleation and assembly. *Nature* 590:416-22
- 136. Takahashi K, Takahashi L. 2019. Data Driven Determination in Growth of Silver from Clusters to Nanoparticles and Bulk. *The Journal of Physical Chemistry Letters* 10:4063-8
- 137. Liu R, Hao J, Li J, Wang S, Liu H, et al. 2020. Causal Inference Machine Learning Leads
 Original Experimental Discovery in CdSe/CdS Core/Shell Nanoparticles. *The Journal of Physical Chemistry Letters* 11:7232-8
- 138. Marx D, Hutter J. 2009. *Ab initio molecular dynamics: basic theory and advanced methods*. Cambridge University Press
- 139. Sun W, Jayaraman S, Chen W, Persson KA, Ceder G. 2015. Nucleation of metastable aragonite CaCO3 in seawater. *Proceedings of the National Academy of Sciences* 112:3199-204

- 140. Behler J. 2014. Representing potential energy surfaces by high-dimensional neural network potentials. *Journal of Physics: Condensed Matter* 26:183001
- 141. Handley CM, Behler J. 2014. Next generation interatomic potentials for condensed systems. *The European Physical Journal B* 87:1-16
- 142. Behler J. 2016. Perspective: Machine learning potentials for atomistic simulations. *The Journal of chemical physics* 145:170901
- 143. Hu Y, Lee B, Bell C, Jun Y-S. 2012. Environmentally abundant anions influence the nucleation, growth, ostwald ripening, and aggregation of hydrous Fe (III) oxides. *Langmuir* 28:7737-46
- 144. Guinier A, Fournet G, Yudowitch KL. 1955. Small-angle scattering of X-rays.
- 145. Porod G, Glatter O, Kratky O. 1982. *Small angle X-ray scattering*. Academic Press, London. 17 pp.
- 146. Choudhary MK, Jain R, Rimer JD. 2020. In situ imaging of two-dimensional surface growth reveals the prevalence and role of defects in zeolite crystallization. *Proceedings of the National Academy of Sciences* 117:28632-9

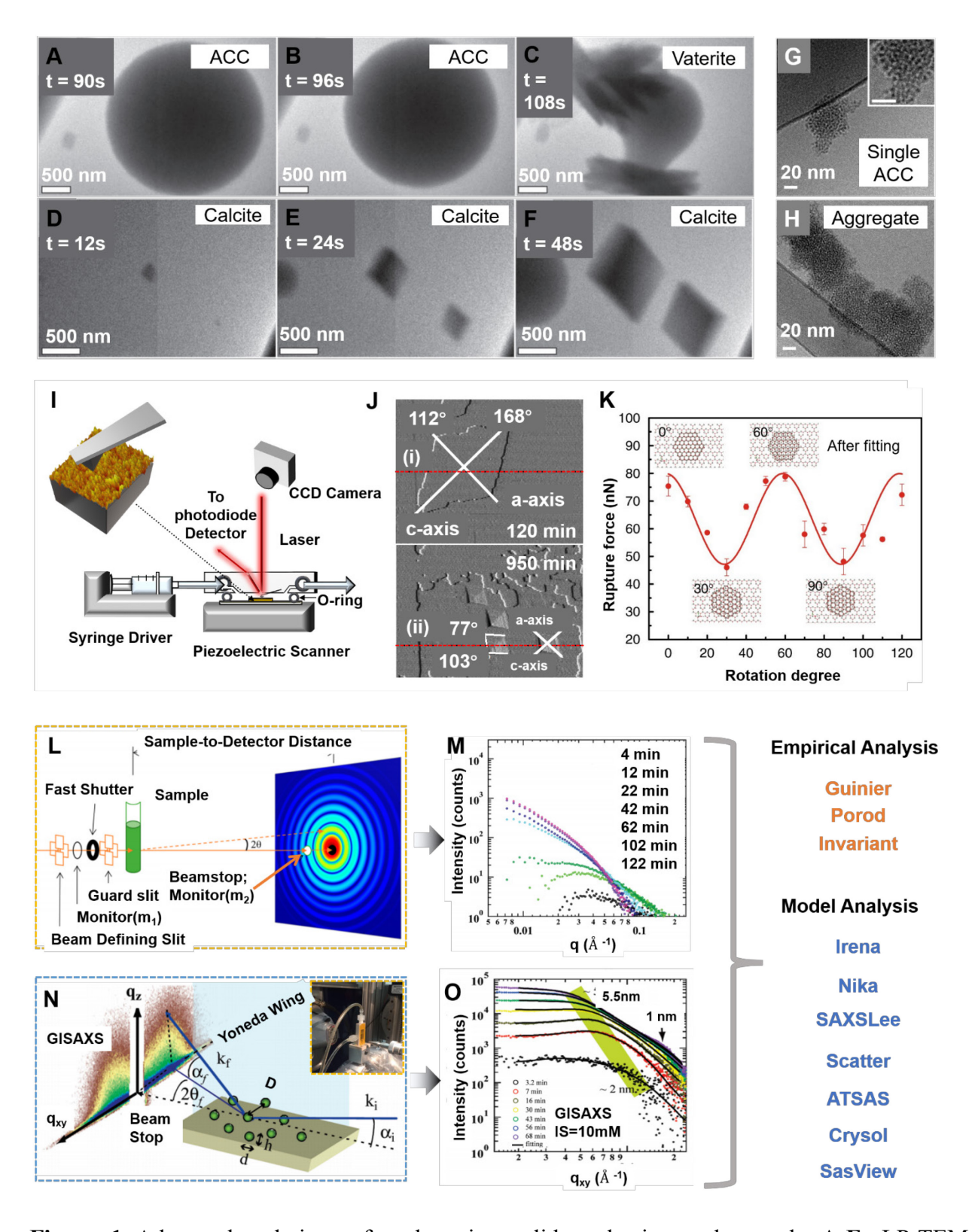


Figure 1 Advanced techniques for observing solid nucleation and growth. **A-F:** LP-TEM observations of phase transformation from ACC to vaterite (**A-C**) and direct calcite nucleation (**D-**

F). Figure adapted with permission from Reference (22); Copyright 2014 American Association for the Advancement of Science. G-H: Cryo-TEM observations of aggregation of ACC caused by poly(aspartic acid). Figure adapted with permission from Reference (23); Copyright 2018 Springer Nature. I: Schematic of fluid-cell AFM; J: The upper AFM figure shows a manganese oxide island formed on manganese carbonate during 120 min exposure to solution; the bottom AFM figure shows simultaneous formation of dissolution pits of manganese carbonate and maganese oxide islands and their coalescence after 950 min. Figure adapted with permission from Reference (24); Copyright 2005 American Chemical Society. K: The rupture forces of the ZnO(0001)– $ZnO(000\bar{1})$ system in aqueous solution at different azimuthal orientations, after modeling fitting. Figure adapted with permission from Reference (30); Copyright 2017, Springer Nature. L: Schematic showing the SAXS system and the 2D scattering data obtained at beamline 12ID-B at the Advanced Photon Source (APS) in Argonne National Laboratory. Figure adapted with permission from Reference (31); Copyright 2016 American Chemical Society. M: A representative 1D SAXS image showing the relationship between the intensity, I, and the scattering vector, q, of a system with homogeneous nucleation of iron(III) (hydr)oxide nanoparticles in solution. Figure adapted with permission from Reference (143); Copyright 2012 American Chemical Society. N: Schematic showing the GISAXS system and the 2D scattering data. Figure adapted with permission from Reference (33); Copyright 2010 American Chemical Society. *Inset*: a picture showing the in situ GISAXS experiment setup at beamline 12-ID-B in APS. Figure adapted with permission from Reference (36); Copyright 2020 American Chemical Society. O: A representative 1D GISAXS figure showing the heterogeneous nucleation of iron(III) (hydr)oxide nanoparticles on quartz at $[Fe^{3+}] = 10^{-4} M$, ionic strength (IS) = 10 mM, and pH 3.6. Nanoparticles formed with a 2 nm radius and grew to a 5.5 nm radius within 70 min; secondary 1 nm radius

particles developed later. Figure adapted with permission from Reference (33); Copyright 2010 American Chemical Society. (Right column) empirical analysis approximations—the Guinier (144), the Porod (145), and the invariant approximation (31); and software packages developed for SAXS data analysis and software packages developed for SAXS data analysis (31): Irena, Nika, simSAXSLee, Scatter, SasView, ATSAS, Crysol.

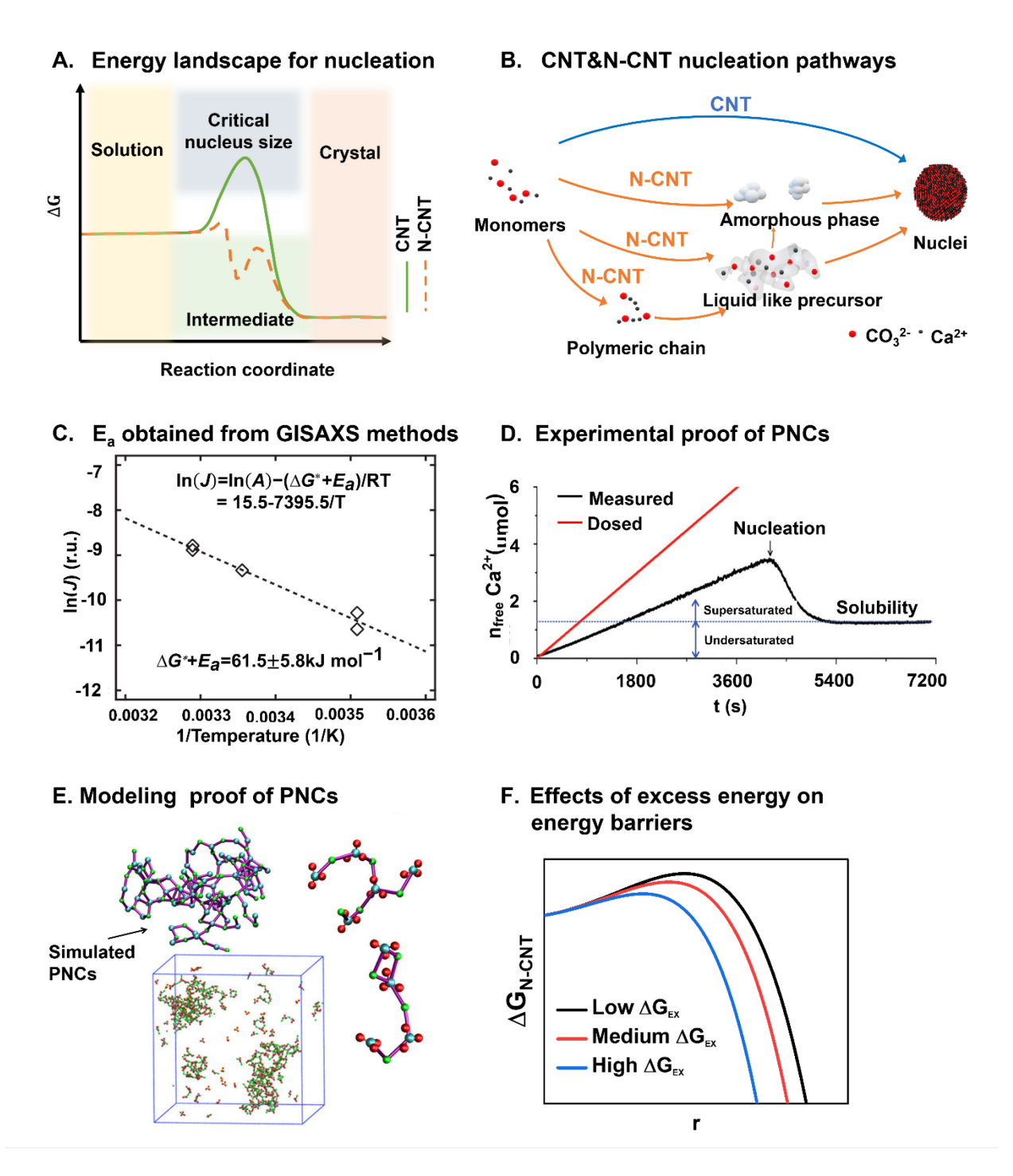


Figure 2. A: Energy landscapes for CNT and N-CNT. **B:** CNT and N-CNT nucleation pathways. **C:** The natural logarithm of nucleation rates $(\ln(J))$ versus 1/temperature, which provides the sum of $(\Delta G^* + E_a)$ from the slope. R is the ideal gas constant (8.314 J mol⁻¹ K⁻¹). Figure adapted with permission from Reference (47); Copyright 2018 Springer Nature. **D:** Comparison of the amounts of calcium ions added (red) and actually detected (black) to determine nucleation rates. Copyright

2008 American Association for the Advancement of Science (52). **E:** Molecular dynamics simulation of calcium (bi)carbonate species at high pH with a snapshot of the simulation box for 0.5 M. Figure adapted with permission from Reference (52); Copyright 2008 American Association for the Advancement of Science. **F:** Incorporation of excess free energy (ΔG_{EX}) can lower the nucleation barrier. Results are obtained from Eq. (3) are calculated based on Reference (59). ΔG_{EX} is related to the interfacial energy of PNCs. Low, medium, and high ΔG_{EX} plots reflect the ratios between the interfacial energy of PNCs and the interfacial energy of nuclei, within the range of 1/8 to 1/15.

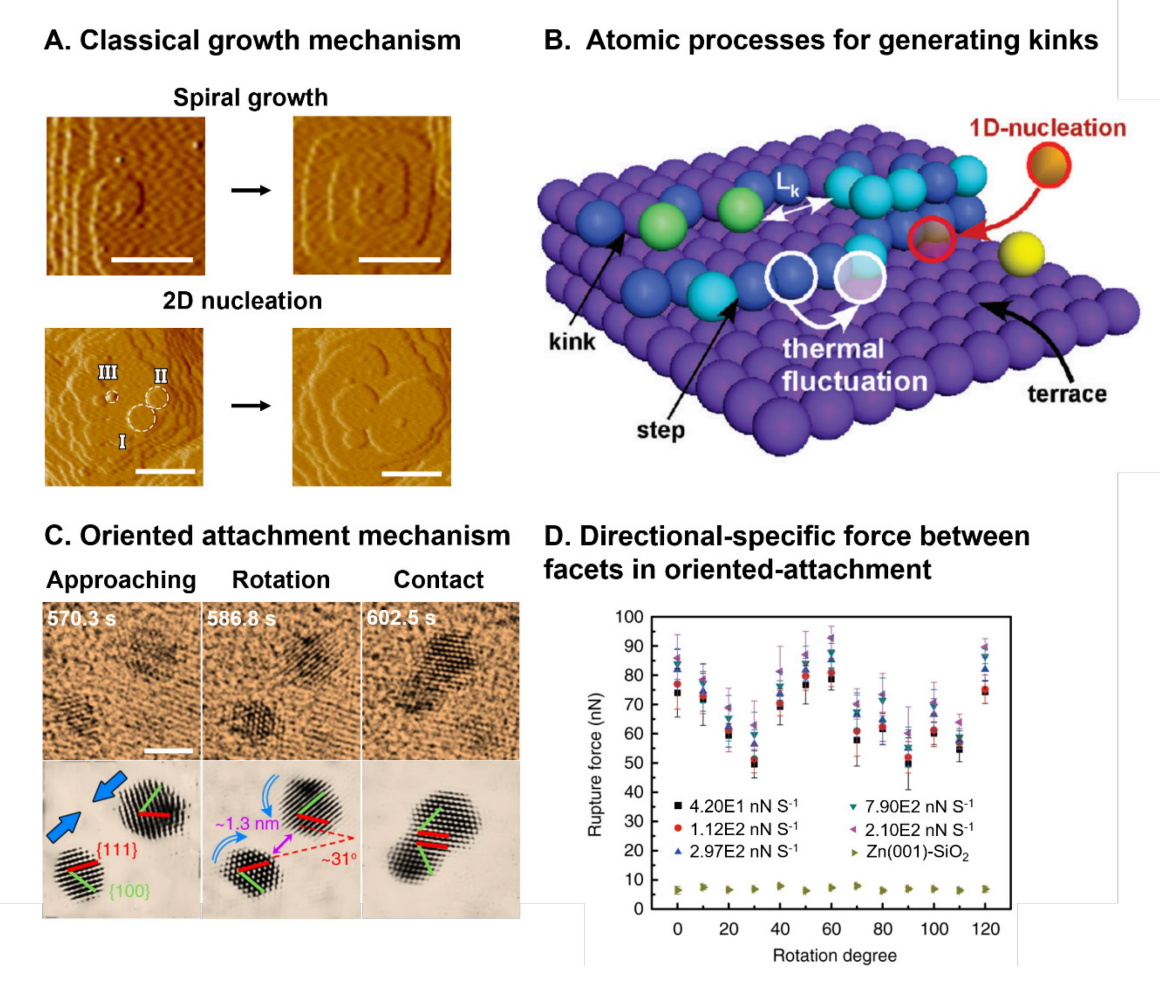


Figure 3 Growth theory and new experimental findings. A: Classical growth mechanisms: spiral growth and 2D island nucleation. Figure adapted with permission from Madhuresh K. Choudhary et al., PNAS, 2020, (146). B: Schematic illustrating terrace, step, and kinks on a crystal surface. Kinks are created either via movements of molecules on the step edge (thermal fluctuations) or attachment of new solute molecules from solution (1D nucleation). Figure adapted with permission from Reference (64); Copyright 2009 American Chemical Society. C: Non-classical growth: In situ TEM measurements revealed the oriented attachment process of gold nanoparticles, including approaching, rotation, and contact. Figure adapted with permission from Reference (72); Copyright 2018 Springer Nature. D: Direction-specific interaction forces at different azimuthal orientations for ZnO(0001)-ZnO(0001) interactions. Rupture force is the jump-from-contact force when the single crystal on the tip is approaching/retracting single crystal substrate. Rotation angle is the azimuthal angle between the single crystal on the tip and single crystal substrate. Figure adapted with permission from Reference (30); Copyright 2017, Springer Nature.

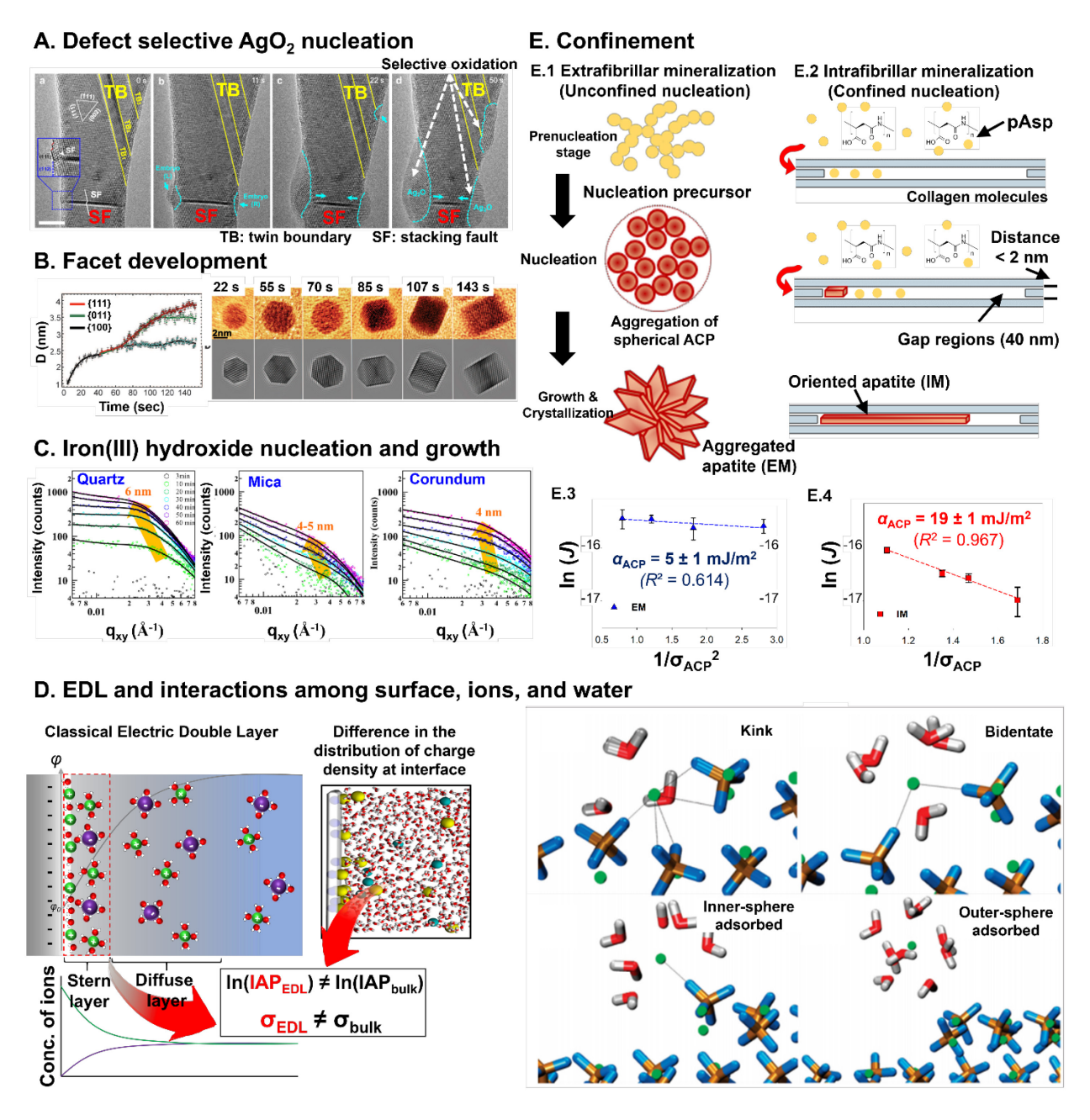
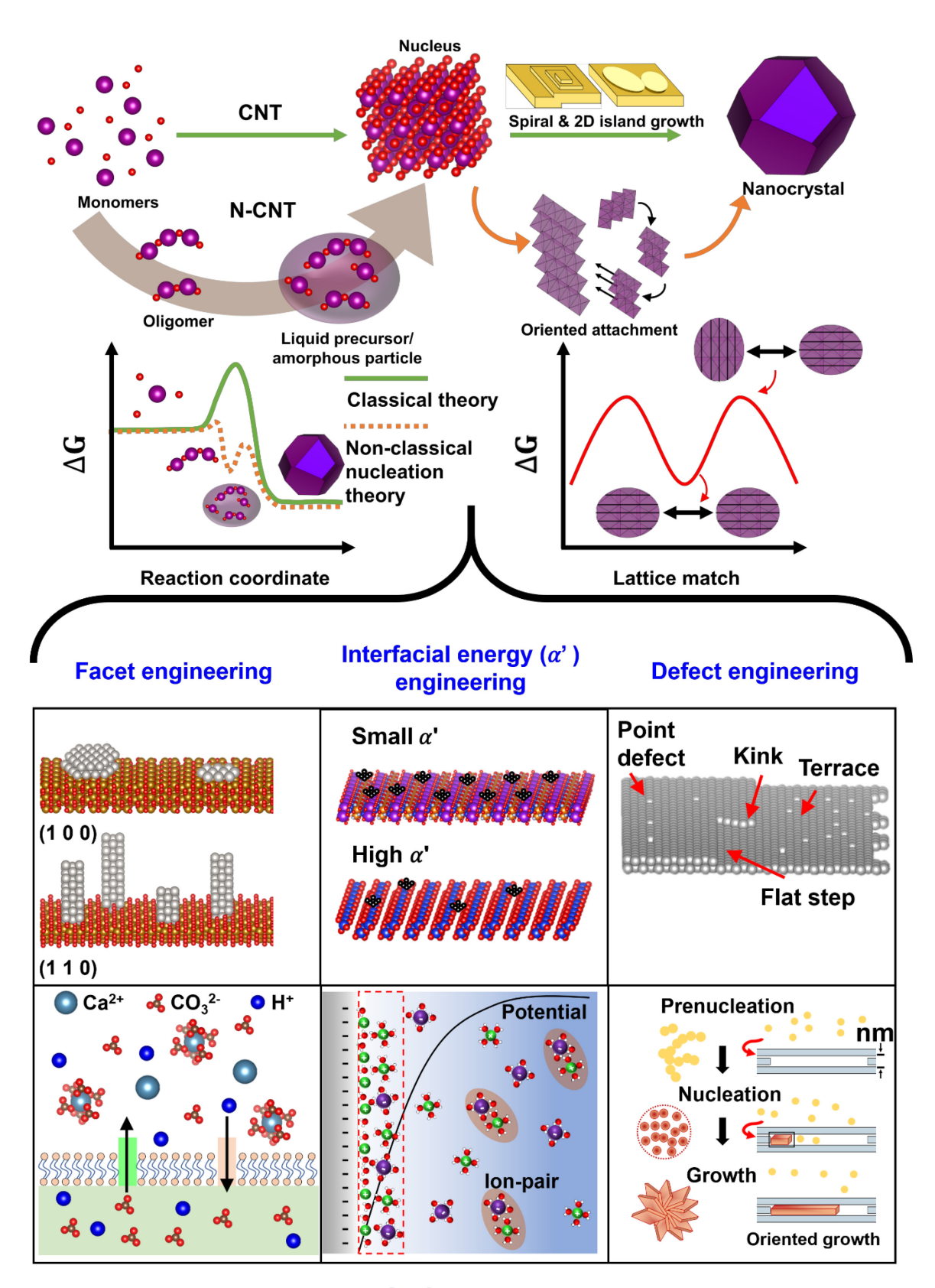


Figure 4. Factors affecting nanoparticle nucleation and growth. **A:** Selective AgO₂ nucleation at different facets of Ag nanocrystals. Figure adapted with permission from Reference (86); Copyright 2021 Springer Nature. **B:** Measured distances from the center of Pt nanoparticles to each facet, directly related to their growth rate, and sequential images of a Pt nanocube's growth. Figure adapted with permission from Reference (90); Copyright 2014 American Association for the Advancement of Science. **C:** Iron(III) (hydr)oxide heterogeneous nucleation on different substrates: quartz, mica, and corundum. Figure adapted with permission from Reference (92);

Copyright 2013 American Chemical Society. **D:** (Left) The formation of an electric double layer (EDL) and inhomogeneous charge distribution at the EDL. In the figure of MD simulation results, yellow and cyan spheres indicate cations and anions, respectively. (Right) MD simulation results were adapted with permission from Reference (101); Copyright 2014 American Chemical Society. Interactions among surface, ions, and water are all important in controlling barite growth kinetics (104): bonding at kink sites, bidentate complexation, inner-sphere complexation, and outer-sphere complexation. Barium atoms are green, sulfate ions are ochre (sulfur) and blue (oxygen), oxygens atoms of water are red and hydrogens are gray. Figure adapted with permission from Reference (104); Copyright 2012 American Chemical Society. **E:** Schematics of two different nucleation models for collagen mineralization. (**E.1**) Extrafibrillar nucleation in unconfined space and (**E.2**) intrafibrillar nucleation in a confined gap region. (**E.3 and E.4**) Interfacial energies for ACP nucleation (α_{ACP}) during EM and IM, calculated from the relationship between *J* and supersaturation (EM: $\ln(J)$ vs $1/\sigma^2$; IM: $\ln(J)$ vs. $1/\sigma$ due to nanoconfinement) (132). Figure adapted with permission from Reference (132); Copyright 2018 Springer Nature.



Bioinspired strategy

Surface charge engineering

Confinement engineering

Figure 5. Perspectives toward a holistic understanding of classical and nonclassical nucleation and growth mechanisms, and determining factors in engineering nanoparticles and understanding their behavior. Theoretical and experimental approaches can yield a comprehensive model connecting the nucleation and the growth behaviors of nanoparticles. Such model development can predict the behavior and formation of nanoparticles more accurately, enabling us to design and predict their properties in engineering fields and nature. The middle left ΔG figure illustrates the free energy landscapes in classical and non-classical nucleation and classical growth pathways. The middle right ΔG figure portrays the free energy landscape during a non-classical growth pathway *via* oriented attachment.